2009 American WJTA Conference and Expo
August 18-20, 2009 • Houston, Texas

Paper

KERF CHARACTERIZATION IN ABRASIVE WATERJET CUTTING

Jay Zeng and Axel Henning
OMAX Corporation
Kent, Washington, USA

ABSTRACT

As the level of precision in abrasive waterjet cutting got higher and higher over the past decade, so has the demand. More and more attention has been paid to the kerf geometry and its dependence on the process parameters. Error compensation using a tilt-able cutting head is becoming popular. A better understanding of the kerf characteristics, coupled with the latest tilting head technology, will further elevate the level of precision.

The article will review what has been reported in the topic of kerf characterization of abrasive waterjet cutting. Furthermore a systematic approach is used to conduct a series of cutting experiments to evaluate the kerf geometry at variation of process specific parameters. The kerf surfaces are scanned with a laser to collect data of kerf geometry and surface profiles. These data will provide additional insight into the kerf characterization in abrasive waterjet cutting.

With this approach the achievable level of accuracy of abrasive waterjet cutting can be taken to a new level allowing this promising technology to propagate into areas of precision machining where it can be used to supplement conventional methods.

Organized and Sponsored by the Waterjet Technology Association

1. INTRODUCTION

Abrasive Waterjets have become a well established cutting tool in many areas of industrial production. Since its first applications comprising of simple separation task in the 1980's it has evolved to become an integral part of many manufacturing processes (Olsen (2009)). Most of today's applications in cutting with abrasive waterjets are found in flexible and reliable two-dimensional separation of flat stock materials. Especially in high precision and near net-shape manufacturing of high alloy steels and light metals lie substantial potentials for development of this innovative technology. With most cutting systems these applications require a high degree of expertise of the operator to implement the necessary adjustments of the tool path and selection of parameters. For this the operator typically consults empirically generated lookup tables to obtain information about the cutting capability of the abrasive waterjet. Advanced cutting models therefore aim at correlating the process parameters with cutting speed, maximum cutting depth and quality of the cutting edge (e.g. Zeng (1992)).

While these approaches significantly improve the usability of the abrasive waterjet cutting, still major geometric deficiencies occur at the cutting edge especially at small radiuses and corners. In mere two-dimensional three-axis cutting the only way to avoid such effects is to significantly reduce the cutting speed at these points, which would result in a wider taper at the bottom of the kerf and thus other deviations from the demanded contour. With conventional cutting changes of the contour shape due to parameter variations have mostly been ignored, limiting the achievable precision of abrasive waterjet cutting. All contour optimization efforts in three-axis machining can therefore only be a compromise between the required accuracy and the demand for high cutting speed for best machining performance. To meet current demands regarding precision of the cutting contour further linear and angular tool path corrections have to be applied and integrated into current software solutions (e.g. Henning (1997 and 2007)).

In order to improve the precision of the contour in metal cutting, tilting kinematics have been developed, which are capable of compensating both taper and jetlag angle without compromising the cutting performance (Zeng et. al. (2005)). With extensive support of comprehensive geometrical cutting models that are implemented in some of the more advanced cutting software the operator can benefit from the improved precision without sacrificing cutting performance. The other resort of improvements can be found in modeling the kerf width characteristic. Similar to the angular compensation approaches the kerf width also strongly depends on all parameters that are involved in the cutting process. A better understanding and modeling of the kerf characteristics, coupled with the latest tilting head technology, will further elevate the level of precision. With its simple integration in recent software the model can support the user to significantly improve precision of his cutting operation.

The development and integration of new approaches to modeling of the abrasive waterjet cutting process has already shown a great potential in optimizing the cutting process and elevating abrasive waterjet cutting to a new level of precision. In industrial environments this will lead to improved performance, reliability and usability of the process which will eventually lead to new applications and thus new markets of this innovative technology.

2. LITERATURE REVIEW

To advance the technology it is important to know what has been done. A literature review on the kerf characterization of abrasive waterjet cutting is done by the following categories:

Category (1): Profile of the Cutting Front and Jetlag

This area of study was pioneered by Hashish (1984). His visualization study by using high-speed camera and transparent workpiece material captured the curve-shape of the cutting front and the cyclic nature of the abrasive waterjet cutting process (Figure 1).

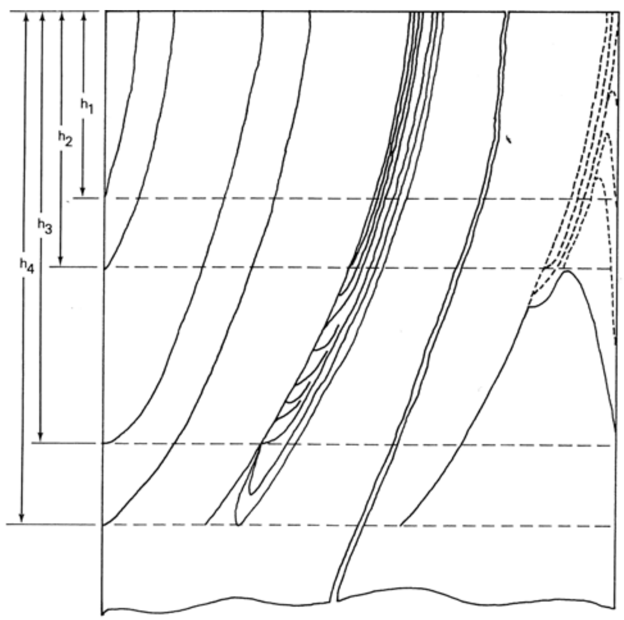

Figure 1. The cutting front and the cyclic nature of the cutting process (Hashish (1984)).

Matsui et al (1990) found that the profile of the cutting front ("dragline") can be represented by an arc with a radius related to the cutting speed as shown in Figure 2. Zeng et al (1991) etched the striation marks on the cut surfaces and found that these striation marks can be well represented by parabolic curves. Jetlag (also called "drag", "cutting lag") is defined as the horizontal lag distance between the bottom and the top of the kerf., measured at the traverse direction. Kitamura et al (1992) showed that jetlag is linearly proportional to the cutting speed while the slope of the line increases with thickness (Figure 3). The experimental data of Hashish (2007) confirmed this observation. Friedrich et al. (2000) proposed a spatio-temporal modeling approach by assuming a moving jet profile in the form of $J=J(r - \lambda e_x t)$, where r is the radial coordinate of the jet, λ the feed rate, e_x the unit vector in the direction of feed, and t the time. It was shown that this approach has the potential to provide more insight into the kerf formation mechanism including the striation phenomenon. Henning et al. (2002) generated a surface scan of an abrasive waterjet cut surface with an auto-focus sensor (Figure 4a). The depth of striation was represented by 6 times of the standard deviation (σ) of each scan and plotted in Figure 4b, indicating a parabolic curve below a straight-line at the upper surface. The cross correlation coefficients between every two neighboring scans were calculated and plotted in Figure 4c. The first maximum of the cross correlation coefficients represents the spatial shift between the two neighboring scans, which were plotted in Figure 4d. Again the straight line (past a zero spatial shift zone (Kc)), representing the spatial shift over the cutting depth, indicates a parabolic shape of the striation curves. Henning and Westkämper (2004) studied the impact of translational and rotary energy of abrasive particles to the curvature of the cutting front. They also presented some results of a 3D jet shape model when cutting a circular path, which agree well with measurements of tested samples. The model was developed based on a test matrix of about 300 steel and aluminum data with variables including radius of the circular path, cutting speed, abrasive flow rate, orifice diameter, and mixing tube diameter. The same authors (in 2006 and 2007) further analyzed the dynamics of the cutting front and showed a time series of local material removal rate along the cutting front based on their spatio-temporal model.

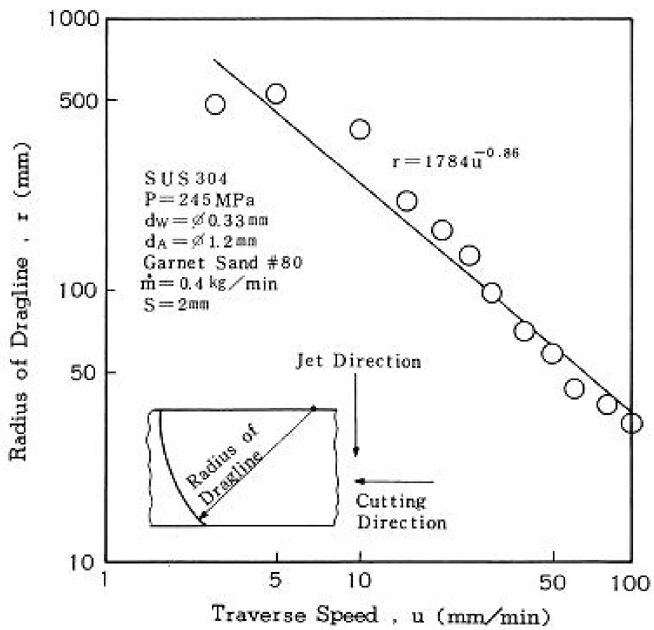

Figure 2. Dragline radius as a function of the cutting speed (Matsui et al (1990)).

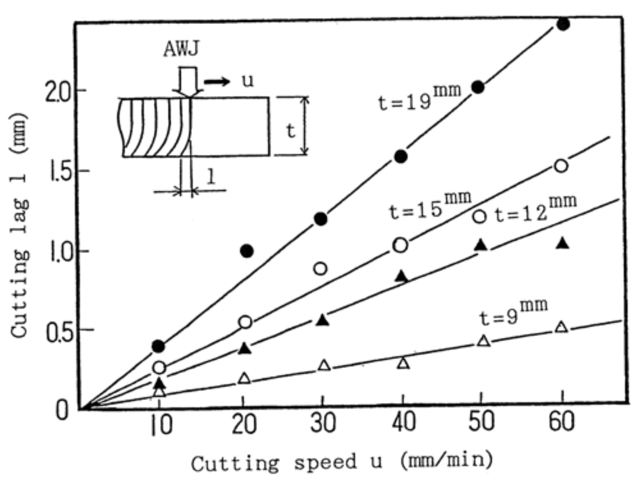

Figure 3. Jetlag vs cutting speeds (Kitamura et al (1992)).

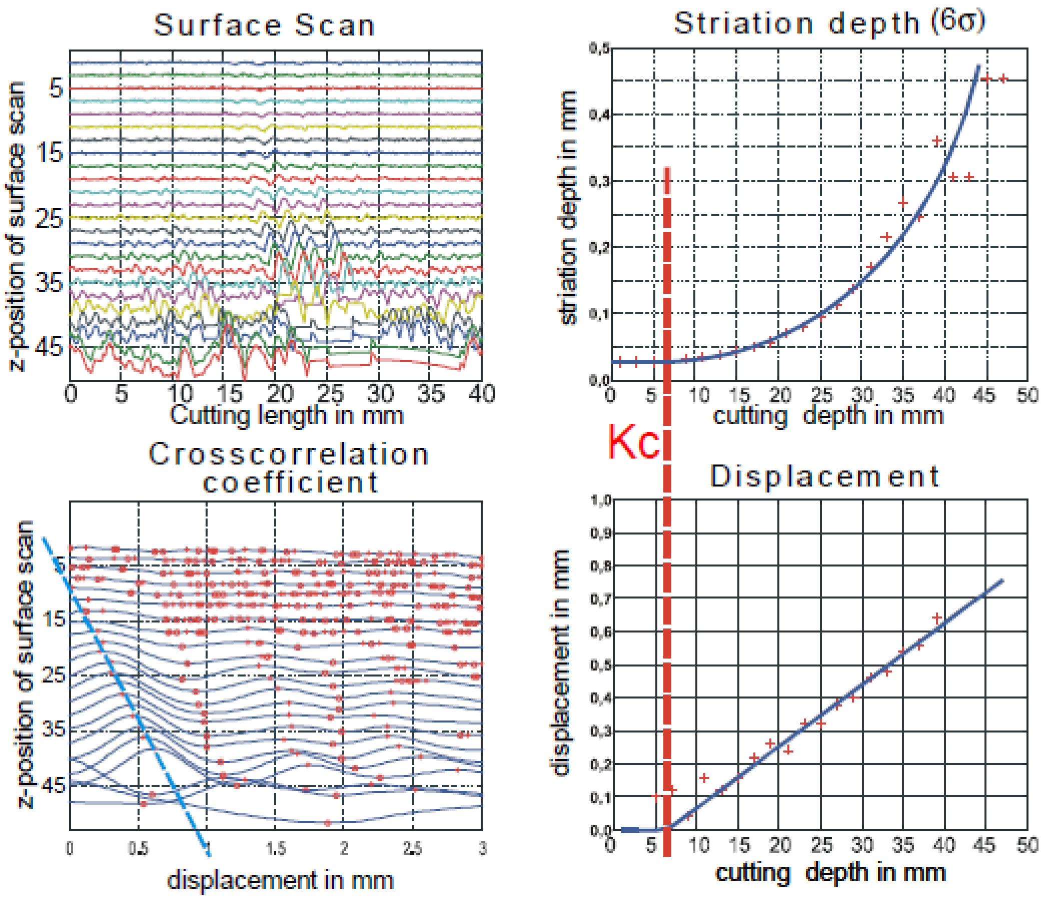

Figure 4. Analysis of striation depth and shape (a) surface scan b) striation depth c) cross-correlation d) displacement) (Henning and Westkämper (2002)).

Category (2): Kerf Width (KW)

An experimental study by Matsui et al (1990) revealed that the kerf width at both the top and bottom sides of the kerf decreases linearly with increasing cutting speed on a semi-log plot (Figure 5).

Capello & Groppetti (1992) used an optical microscope to measure the kerf width at different heights of a non-through cut and constructed the kerf shape, by assuming it is symmetric, as shown in Figure 6. They found that the kerf shape is relatively independent of the water pressure and abrasive flow rate, but is strongly influenced by the standoff distance and abrasive grain size.

Chung et al (1992) came up with some single-factor linear regression equations to link kerf width to mixing tube diameter, abrasive flow rate, and stand-off distance. Henning & Anders (1998) found that, as long as the material, the cutting speed, and other jet parameters remain the same, for samples with different thicknesses, the kerf profiles overlap with each other until the depth is large enough that the deviation caused by the striation marks starts to show (see Figure 7).

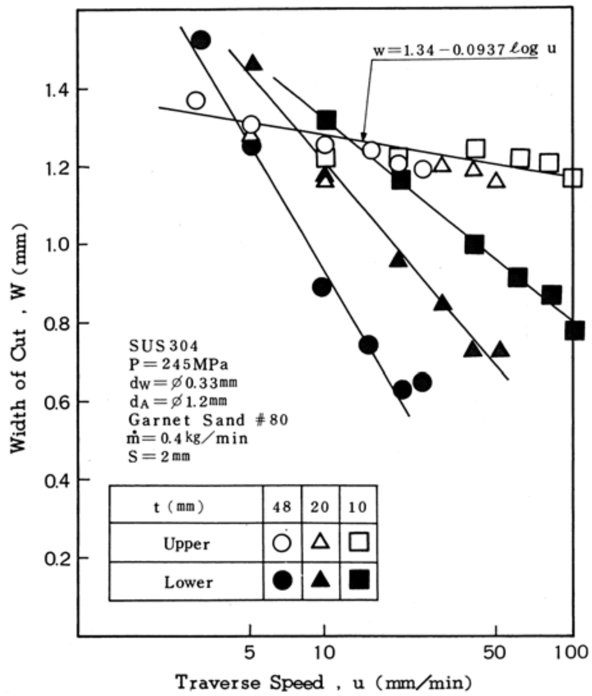

Figure 5. Relation of kerf width vs cutting speed (Matsui et al (1990)).

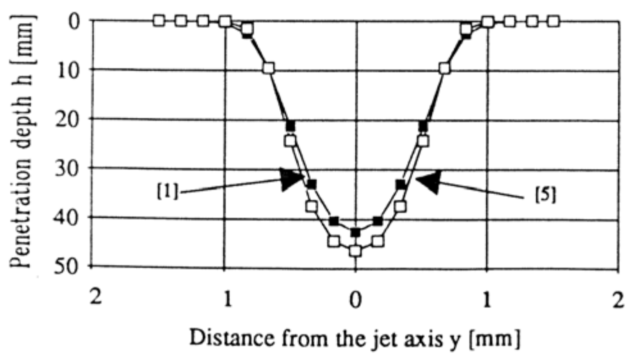

Figure 6. Kerf shape of a non-through cut (Capello & Groppetti (1992)).

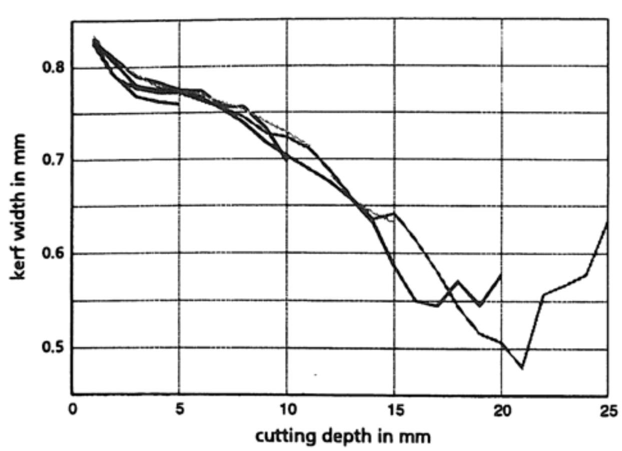

Figure 7. Kerf profiles with different thicknesses (Henning & Anders (1998)).

Henning and Westkämper (2000), as well as Westkämper et al (2000), investigated the contributions of primary impact and secondary impact of the jet to the kerf formation by measuring the kerf profile formed on a thin sheet metal with an image processing coordinate measuring machine (Figure 8).

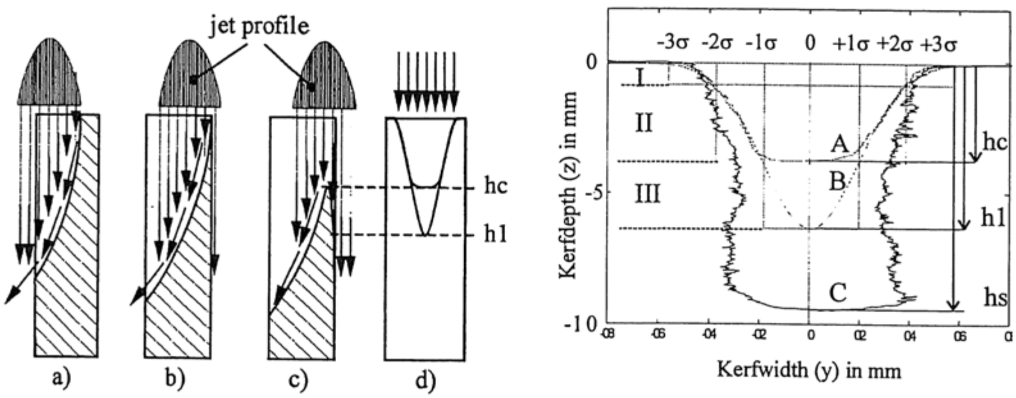

Figure 8. Kerf profile formed on a sheet metal specimen (Henning and Westkämper (2000)).

Category (3): Taper (TE)

Taper error is defined as half of the difference between the top and bottom kerf width. Taper angle is the arctangent of taper error over thickness. Figure 5 (by Matsui et al (1990)) implies that taper error has a linear relationship with the logarithm of the cutting speed. Some single-factor linear regression equations were presented by Chung et al (1992) to link taper to mixing tube diameter, cutting speed, and stand-off distance. Groppetti et al (1998) derived a taper model based on the assumption of the input energy being dissipated along the thickness. In this model, the taper angle (TA) is expressed by:

$$TA = \frac{KW}{h} - C_3 \cdot h^{C_1 - 1} \cdot \frac{AR \cdot P}{2 \cdot U} \left(\frac{WR}{WR + AR} \right)^2 \qquad (1)$$

where h is the thickness of workpiece, P water pressure, U cutting speed, KW kerf width, WR and AR water mass flow rate and abrasive mass flow rate, respectively, and C_1 and C_3 two coefficients. Annoni and Monno (2000) obtained an empirical equation of taper, based on multiple linear regression, as:

$$TE = 1.095 \frac{MD^{0.00453} \cdot AM^{0.0452} \cdot U^{0.0849}}{AR^{0.0321} \cdot P^{0.0765}} - 1 \qquad (2)$$

where MD is the mixing tube diameter and AM abrasive mesh number. Hashish (2007) showed experimental data that indicates that taper angle increases with the cutting speed until about 80% of the maximum speed. Maccarini et al (2008) found that taper increases with the hardness of workpiece material as well as the cutting speed.

Category (4): Barrel Error

Matsui et al (1990) showed, in Figure 9, the kerf profiles as a function of the cutting speed. Barrel error is defined as the straightness error of the kerf on the thickness coordinate. It measures the maximum deviation of the kerf profile from a base line connecting the top and bottom edges of the kerf. The curvature changes from convex to concave as the cutting speed decreases. The straightest profile occurs at the mid speed range.

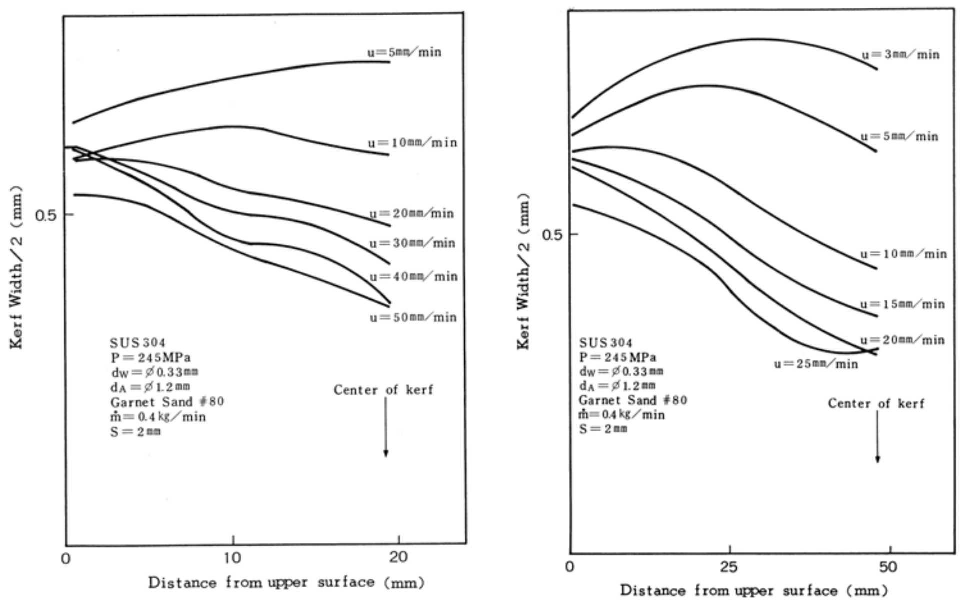

Figure 9. Kerf profiles (Matsui et al (1990)).

Category (5): Surface Roughness and Waviness

Matsui et al (1990) also reported surface roughness data as a function of the cutting speed in Figure 10. The plot on the left shows that the roughness on the upper and middle sections of the thickness is relatively independent of the cutting speed, but the roughness on the lower section increases significantly with the cutting speed. The plot on the right shows that the roughness on the lower sections for three different thicknesses can be represented with a single function of the normalized cutting speed. Many more papers have been published on this topic. Reviewing all of them is outside the scope of this paper and will be reserved for the future.

Category (6): Burr

Burr is typically formed at the bottom edge of the kerf. Groppetti & Monno (1992) dedicated a study towards burr formation in abrasive waterjet cutting and concluded that the formation of a plastic hinge is the basic burr-forming mechanism. They classified this type of burr as a rollover type. Their data show a linear dependence of the burr height on the cutting speed. Groppetti et al

(1998) added more details to their previous study in 1992. Figure 11 shows some SEM photographs of burrs at different cutting speeds.

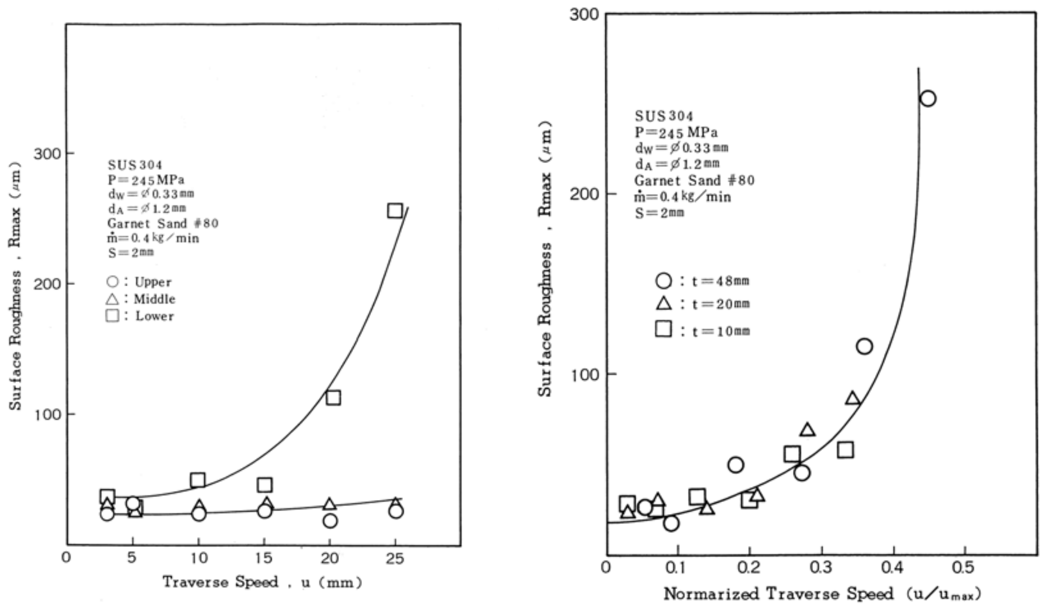

Figure 10. Surface roughness (Rmax) as a function of the cutting speed (Matsui et al (1990)).

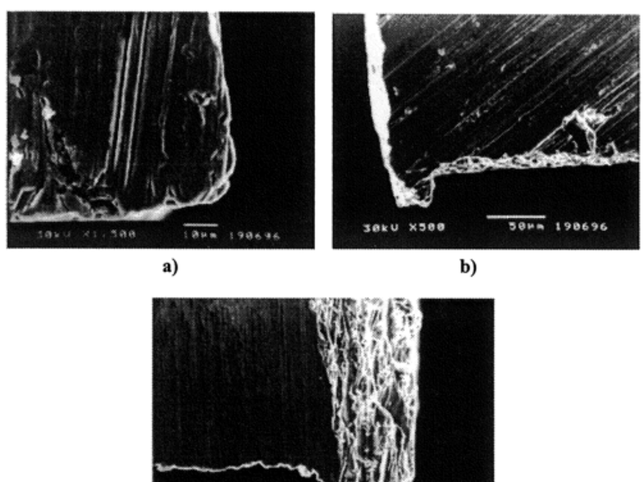

Figure 11. Burr morphology on AISI 304 sample, obtained at: a) suitable feed rate, b) low/medium feed rate, c) high feed rate (Groppetti et al (1998)).

Category (7): Entrance Radius

Groppetti et al (1998) also studied the entrance rounding that is typically present on the top edge of the kerf. Figure 12 shows a SEM photograph of a typical rounded edge (left) and the measured radius as a function of the cutting speed (right) on an AISI 304 sample.

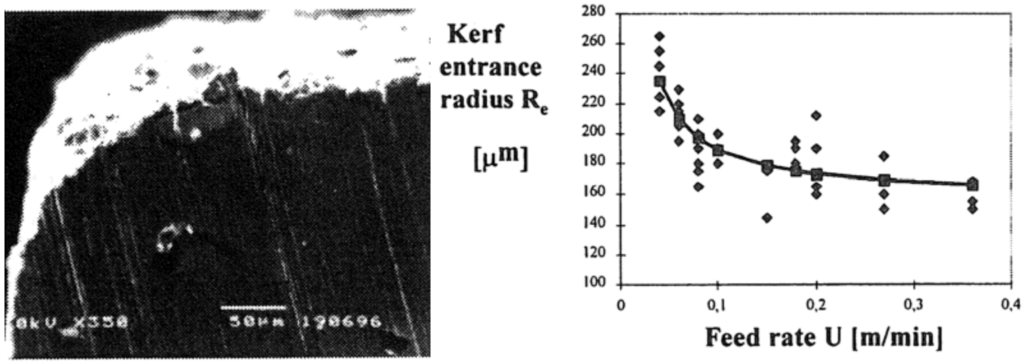

Figure 12. A SEM photograph of a typical rounded edge (left) and the measured radius as a function of the cutting speed (right) (Groppetti et al (1998)).

Based on these data they obtained the following regression equation:

$$R_e = 157.92 + \frac{3.12}{U} \tag{3}$$

where R_e is the entrance radius and U the cutting speed.

3. EXPERIMENTAL STUDY

3.1 Test Conditions and Procedure

Tests are conducted to reveal the impacts of cutting speed, material thickness, and nozzle size to various kerf characteristics. The test conditions are listed in Table 1. For each of these tests, first of all, trial cuts were done to determine the separation speed (i.e. the maximum speed that cuts through the sample completely). Then a straight-line cut of 50 mm long was done with the traverse speed varying linearly from start to end (between two pre-drilled holes so that the sample remains un-separated for the purpose of kerf width measurements). According to the cutting model by Zeng et al (1992), the cutting speed is related to a quality index Q as follows:

$$U = U_{sep} / Q^{1.15} \tag{4}$$

where U_{sep} is the separation speed. In these test cuts, the end speed is set to the same as the separation speed (i.e. Q=1) and the start speed is set to 7.08% of separation speed (i.e. Q=10), the so-called Q10 speed.

3.2 Data Collection and Processing

A laser profile scanner (Cobra brand) by QVI was used to scan the top of the kerf at 13 equally spaced points along the 50 mm cut length to produce a series of profiles like the one shown in Figure 13. A Matlab program was written to automatically determine the kerf width from the scanned data (as shown, in inches). Kerf width data for the samples cut with the 0.508/1.067 mm (0.014"/0.030") nozzle are shown in the semi-log plot in Figure 14. Here the cutting speeds have been converted to the Q index with equation (4). The linear regression fit for all the three curves suggests a relation between kerf width and the logarithm of the Q index (and thus the cutting speed) similar to that shown in Figure 5 by Matsui et al (1990).

Table 1. Test parameters (common conditions: Al6061-T6 samples, 380 MPa pump pressure)

Test	Sample Thickness	Abr. Mesh	Orifice Dia.	Mix. Tube Dia	Abr. Flow Rate	Separation Speed	Start Speed	End Speed
ID	mm		mm	mm	kg/min	cm/min	cm/min	cm/min
1	6.35	80	0.356	0.762	0.392	214.16	15.16	214.16
2	25.40	80	0.356	0.762	0.388	42.06	2.98	42.06
3	50.80	80	0.356	0.762	0.388	15.44	1.09	15.44
4	6.35	50	0.356	1.067	0.591	215.90	15.28	215.90
5	25.40	50	0.356	1.067	0.591	43.18	3.06	43.18
6	50.80	50	0.356	1.067	0.591	16.92	1.20	16.92
7	6.35	50	0.381	1.067	0.591	160.02	11.33	160.02
8	25.40	50	0.381	1.067	0.591	42.35	3.00	42.35
9	50.80	50	0.381	1.067	0.591	17.09	1.21	17.09
10	6.35	50	0.508	1.067	0.729	294.89	20.88	294.89
11	25.40	50	0.508	1.067	0.729	64.21	4.55	64.21
12	50.80	50	0.508	1.067	0.729	26.11	1.85	26.11
13	6.35	120	0.254	0.533	0.222	123.22	8.72	123.22
14	25.40	120	0.254	0.533	0.222	26.66	1.89	26.66
15	50.80	120	0.254	0.533	0.222	9.08	0.64	9.08
16	6.35	120	0.178	0.381	0.152	79.81	5.65	79.81
17	25.40	120	0.178	0.381	0.152	13.97	0.99	13.97
18	50.80	120	0.178	0.381	0.152	4.83	0.34	4.83

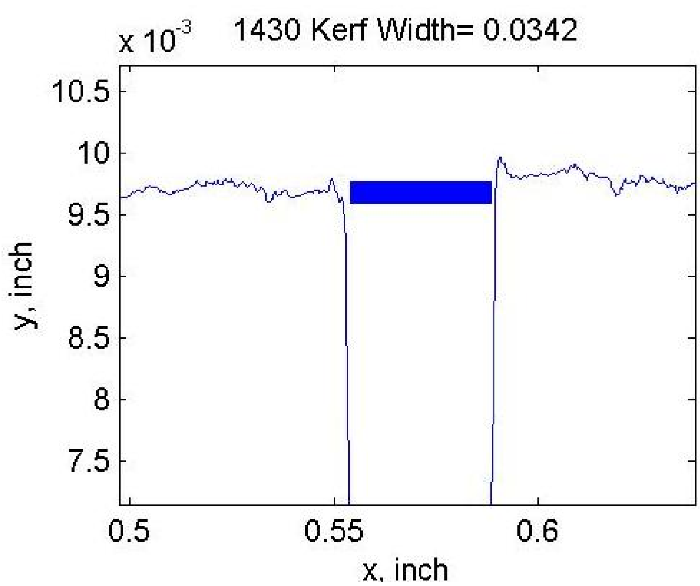

Figure 13. Laser scanned profile on top of kerf.

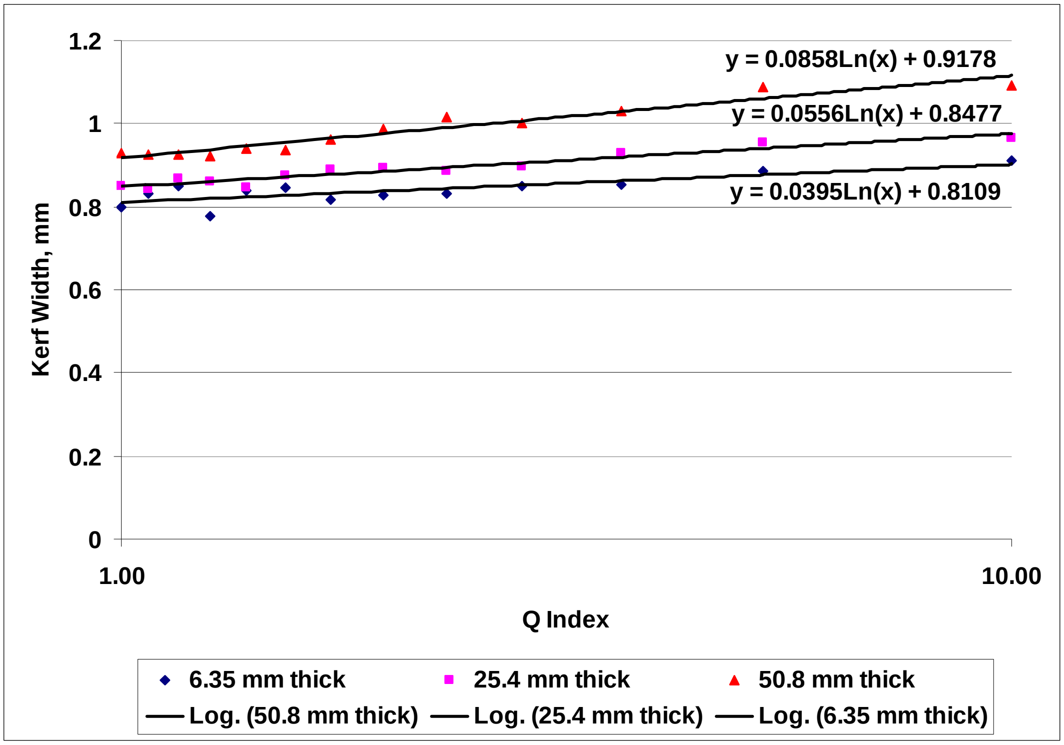

Figure 14. Kerf width measured on top of kerfs for samples cut with 0.508/1.067 nozzle.

Then the sample was cut open with wire EDM to expose the kerf surfaces. Again laser scanning was done on both sides of the kerf walls at multiple heights. A typical profile is shown on Figure 15a (with the horizontal axis being the 50 mm cut length and the vertical axis being the surface profile height in inches for all 4 plots). There are roughly 10,000 data points for a single profile. They were divided into multiple segments along the 50 mm cut length, with 500 data points for each segment. A Matlab program was written to calculate the Ra roughness (Figure 15b) and standard deviation (Figure 15c) for each segment. A linear regression equation represents the roughness profile (shown as a straight dashed line in the plot). A polynomial regression curve of the raw data is shown in Figure 15d, with a dashed line above it representing 2 times of the standard deviation. The dashed line is taken as the macro surface profile, representing a surface measurable with a conventional dimension-measurement tool like a micrometer.

3.3 Results and Discussions

There are multiple linear regression equations of Ra along the thickness coordinate. Connecting all these regression equations vertically forms the roughness profile along the thickness coordinate. Plotting all these roughness profiles together results in one of the plots in Table 2. The curve on the top represents the roughness profile of the maximum speed while the bottom one that of the Q10 speed. The spreading of the curves indicates the variation of roughness caused by the variation of the cutting speed. There is one plot for each nozzle combination and each thickness. All the plots share the same vertical axis scale from -0.0127 mm to 0.0635 mm and the horizontal axis scale from 0 to the full thickness.

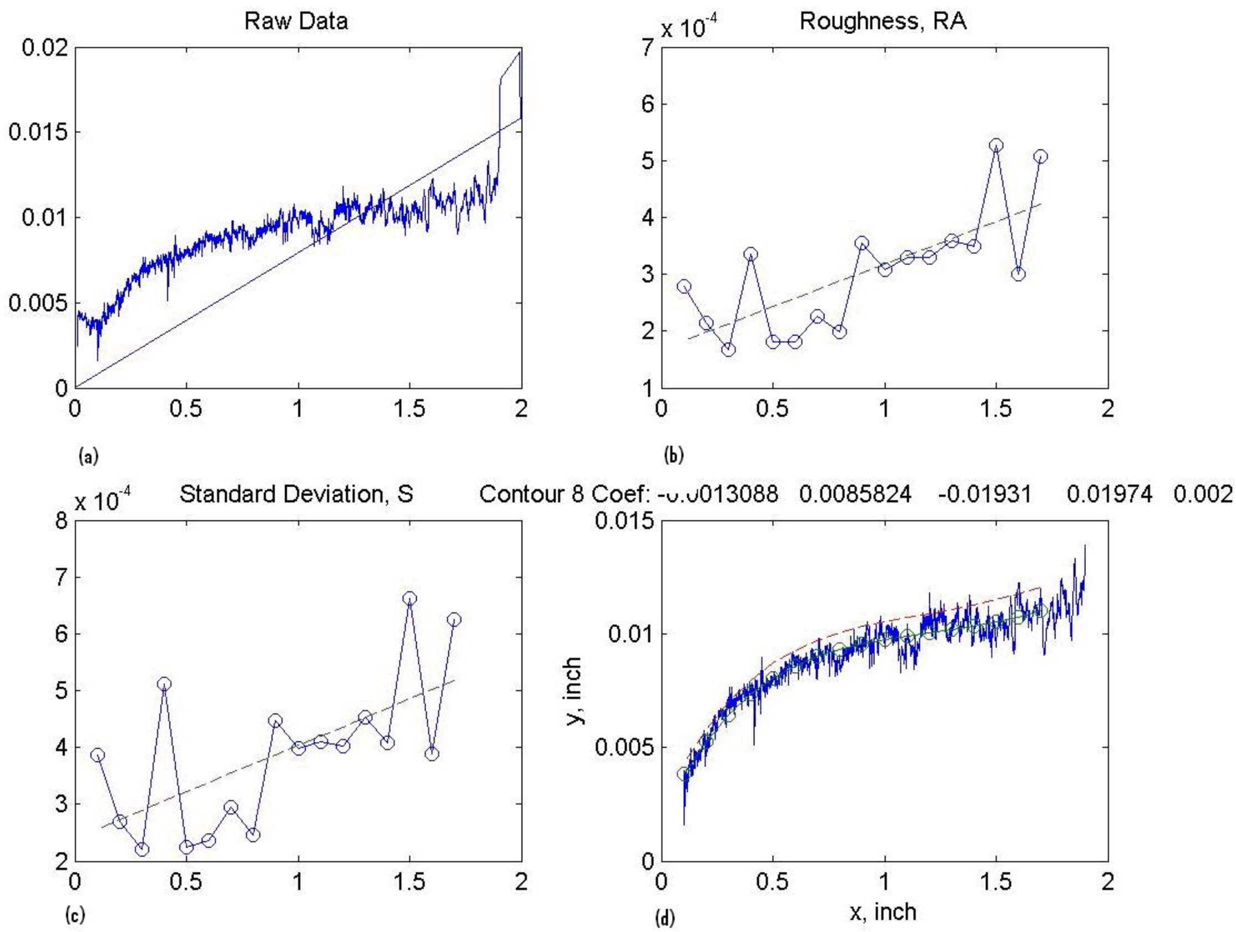

Figure 15. One of the scanned profiles on one side of the kerf.

It is easy to notice that the roughness variation versus cutting speed on the upper part of the thickness is much smaller than the lower part, especially for the 50 mm and 25 mm samples. A logical explanation is that the upper part is cut by the primary impact of the jet while the lower part by the secondary impact. The surface profiles of the lower part reflect the waviness of the striation marks, which is affected much more significantly by the cutting speed. It appears that the thinner samples (6.35 mm) have greater roughness than the thicker ones (25.4 mm and 50.8 mm). The raw data of these thinner samples show evidences of vibration of the part which is more pronounced with higher cutting speeds associated with the thinner samples. It also appears that the bottom part of the samples has lower roughness values than the upper part when the cutting speed is at or close to the maximum. This is an artifact from curve-fitting.

Similarly there are multiple macro surface profiles, represented by the dashed line in Figure 14d, along the thickness coordinate. Connecting all these dashed lines vertically forms the kerf profile along the thickness coordinate. Plotting all these kerf profiles together forms one of the plots in Table 3. The curve at the bottom represents the kerf profile of the maximum speed while the top one that of the Q10 speed. The spreading of the curves indicates the evolution of the kerf shape caused by the change of the cutting speed. There is one plot for each nozzle combination and each thickness. All the plots share the same vertical axis scale from 0 to 1.524 mm and the horizontal axis scale from 0 to full thickness.

Table 2. Surface Roughness Ra vs Cutting Speed
(vertical axis scale from -0.0127 to 0.0635 mm and horizontal axis scale from 0 to full thickness)

Orifice mm (inch)	0.178 (.007”)	0.254 (.010”)	0.356 (.014”)	0.356 (.014”)	0.381 (.015”)	0.508 (.020”)
Mix . Tube mm (inch)	0.381 (.015”)	0.533 (.021”)	0.762 (.030”)	1.067 (.042”)	1.067 (.042”)	1.067 (.042”)
6.35 mm (0.25”) Thick	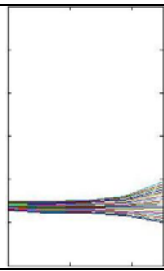	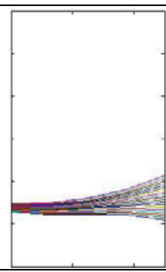	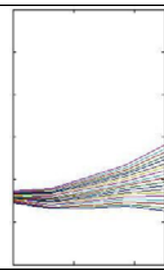	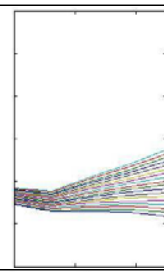	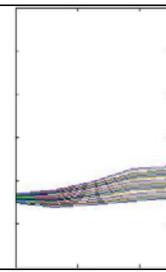	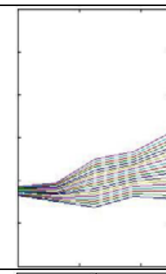
25.4 mm (1”) Thick	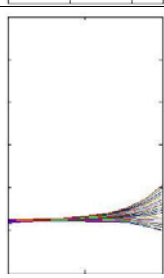	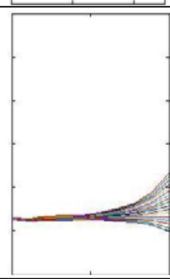	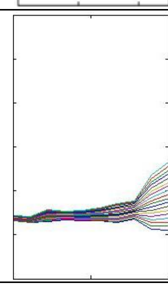	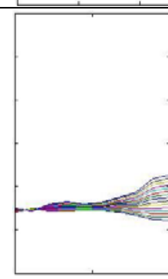	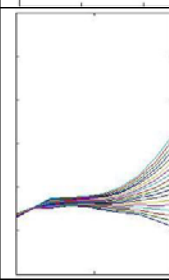	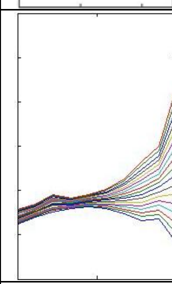
50.8 mm (2”) Thick	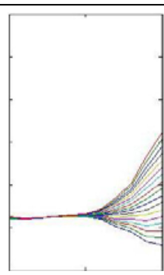	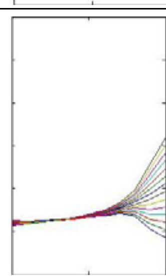	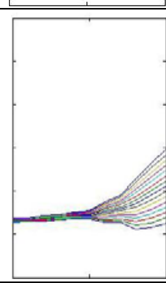	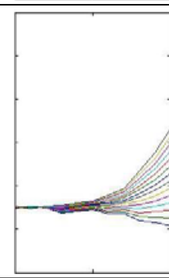	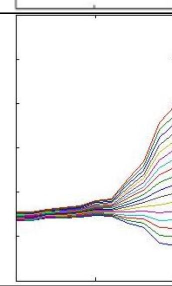	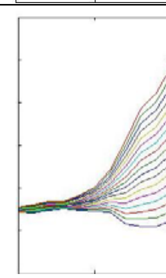

It appears that the taper angle increases with the nozzle size, especially for the thinner samples. It is possible to produce a zero-taper sample by using the proper speed. For the thinner samples, this zero-taper speed is close to the Q10 speed, especially for the larger nozzles. For the thicker samples, the zero-taper speed is at the mid-range.

Based on the macro surface profile models shown in Table 3, the taper errors can be calculated. By converting the cutting speed to the Q index, the taper errors were plotted against the values of log(Q) for all the nozzle combinations and thicknesses. Shown in Table 4 are the three semi-log plots for the 0.356 mm/0.762 mm (0.014”/0.030”) nozzle combination. It was found that the relation between taper error and log(Q) can be represented by two straight lines. The intersecting points of these two straight lines are between Q3 and Q4. It is possible to use a single straight line if representation of the data below Q3 is considered less important. A relation similar to that shown in Figure 5 (by Matsui et al (1990)) will be obtained, i.e.

$$TE = A \cdot \log(Q) + B \tag{5}$$

The coefficients A and B for all nozzle combinations and thicknesses are plotted in Figure 16. A strong correlation between these two coefficients and thickness can be observed.

Table 3. Half Kerf Profiles vs Cutting Speed
(vertical axis scale from 0 to 1.524 mm and horizontal axis scale from 0 to full thickness)

Orifice mm (inch)	0.178 (.007")	0.254 (.010")	0.356 (.014")	0.356 (.014")	0.381 (.015")	0.508 (.020")
Mix . Tube mm (inch)	0.381 (.015")	0.533 (.021")	0.762 (.030")	1.067 (.042")	1.067 (.042")	1.067 (.042")
6.35 mm (0.25") Thick	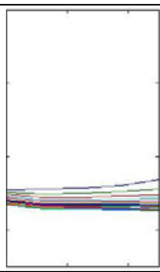	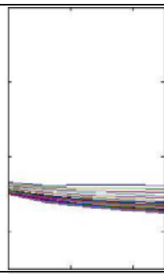	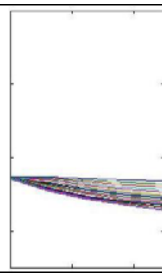	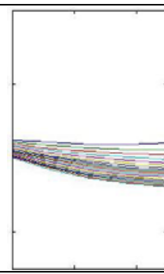		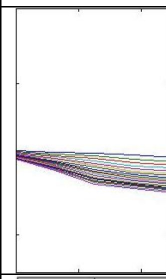
25.4 mm (1") Thick	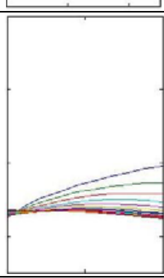	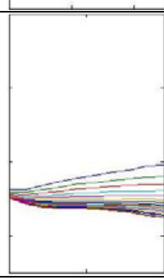	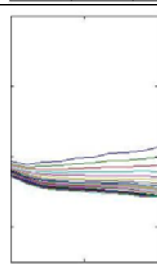	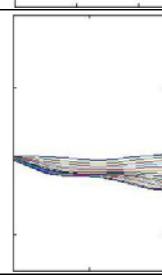	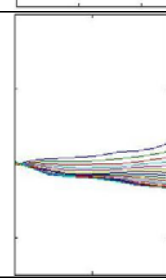	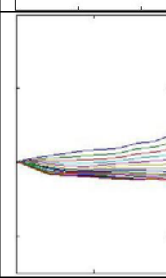
50.8 mm (2") Thick	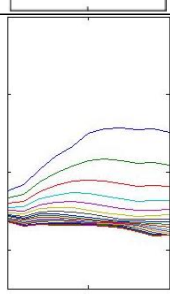	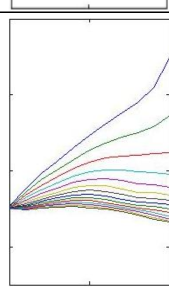	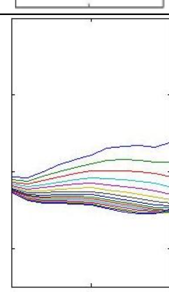	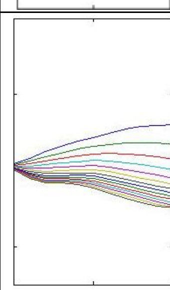	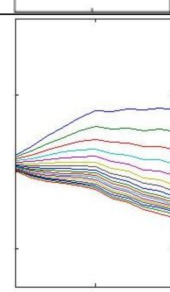	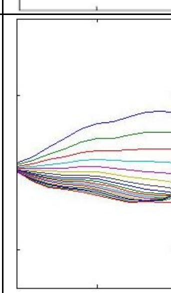

Table 4. Taper Error (TE) vs Log(Q)
(vertical axis scale from -1.016 mm to 0.381 mm and horizontal log axis scale from Q1 to Q10)

Orifice /Mix. Tube mm (inch)	Thickness Mm (inch)	Taper Error Per Side (vertical axis scale from -1.016 mm to 0.381 mm) vs Q Index (horizontal log axis scale from 1 to 10)
0.356 /0.762 (.014" /.030")	6.35 (0.25")	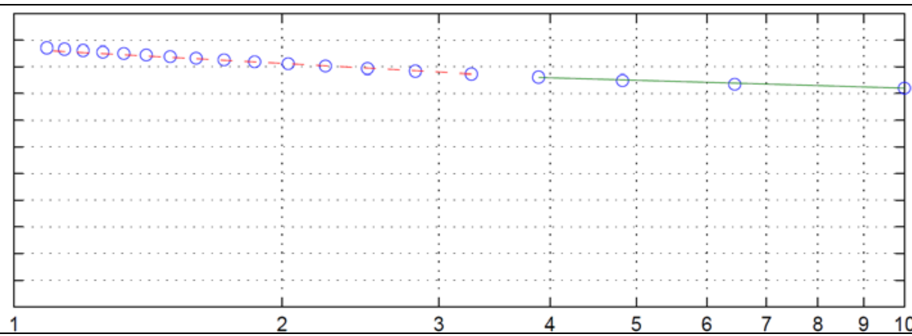
	25.4 (1")	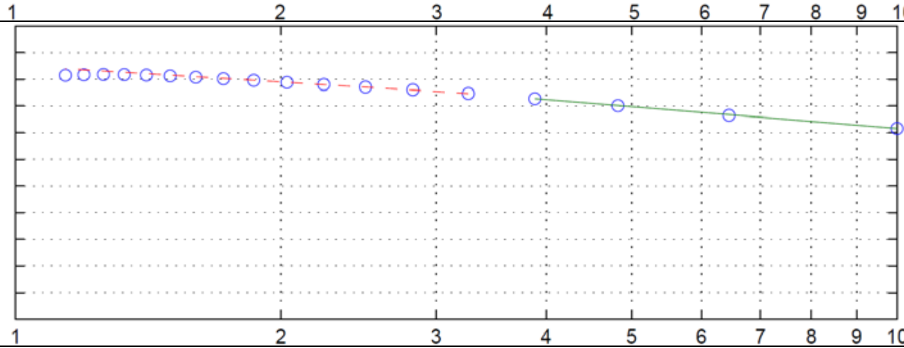
	50.8 (2")	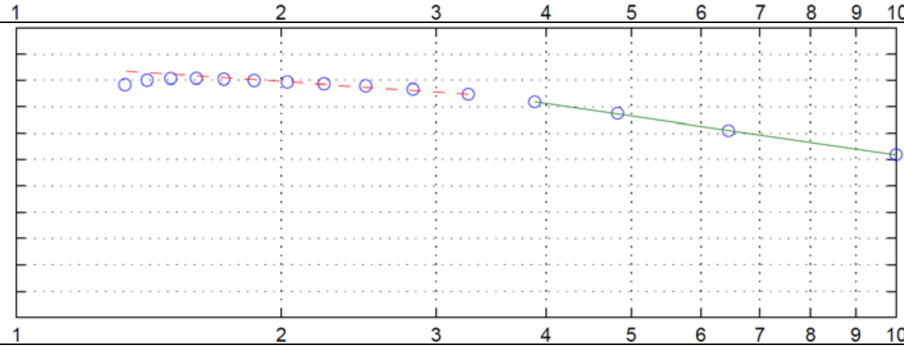

4. CONCLUSIONS

1) Kerf width is linearly proportional to the logarithm of the Q index (and thus the cutting speed).
2) Roughness profile suggests a transitional point that may separate the primary and secondary impact zones.
3) Taper angle increases with nozzle size, especially for thin parts. A zero-taper speed can be found, depending on nozzle size and material thickness.
4) Taper error is also linearly proportional to the logarithm of the Q index (and thus the cutting speed). The two regression coefficients have a strong correlation with thickness.

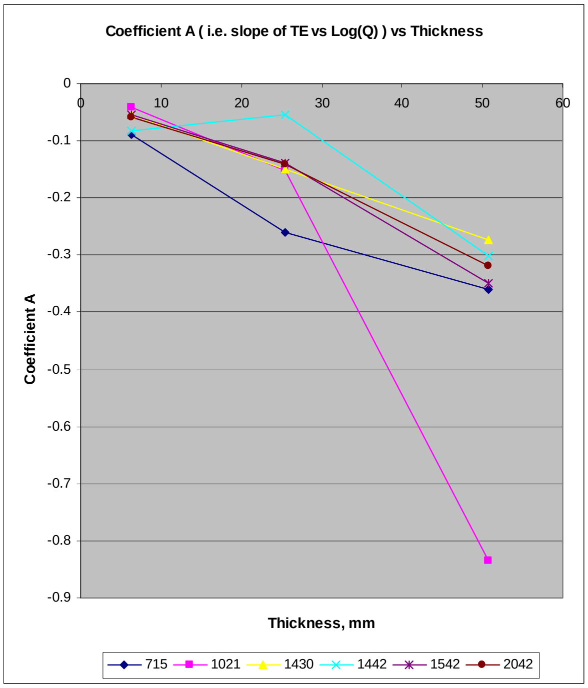

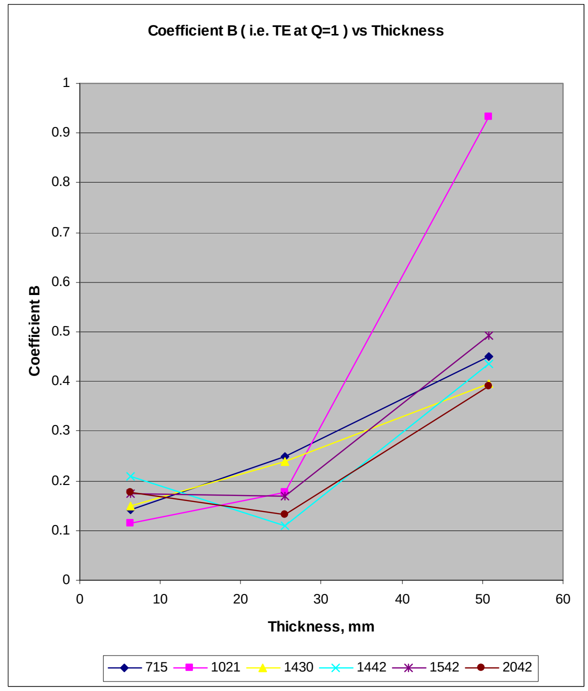

Figure 16. Coefficients of the linear regression of Taper Error=A·log(Q)+B.

5. ACKNOWLEDGMENTS

The authors are thankful to OMAX Corporation management for permission of publishing this paper.

6. REFERENCES

Annoni, M. & Monno, M. (2000) "A lower limit for the feed rate in AWJ precision machining", in Proceedings of the 15th International Conference on Jetting Technology, Ronneby, Sweden, September 6-8, pp 285-296.

Blickwedel, H., Guo, N.S., Haferkamp, H., & Louis, H. (1990) "Prediction of abrasive jet cutting performance and quality", in D. Saunders (Ed.), Jet Cutting Technology - Proceedings of the 10th International Symposium, Amsterdam, The Netherlands, October 31 - November 2, pp 163-179.

Capello, Edoardo & Groppetti, Roberto (1992) "On an energetic semi-empirical model of hydro-abrasive jet material removal mechanism for control and optimization", in A. Lichtarowicz (Ed.), Jet Cutting Technology - Proceedings of the 11th International Conference on Jet Cutting Technology, St Andrews, Scotland, September 8-10, pp 101-120.

Chung, Y., Geskin, E.S., & Singh, P.J. (1992) “Prediction of the geometry of the kerf created in the course of abrasive waterjet machining of ductile materials”, in A. Lichtarowicz (Ed.), Jet Cutting Technology - Proceedings of the 11th International Conference on Jet Cutting Technology, St Andrews, Scotland, September 8-10, pp 525-541.

Friedrich, R., Radons, G., Ditzinger, T., Henning, A. (2000)." Ripple formation through a convective instability from moving and erosion sources", In: Physical review letters 85 (2000), Nr. 23, pp. 4848-4887

Groppetti, R., Gutema, T., & Di Lucchio, A. (1998) “A contribution to the analysis of some kerf quality attributes for precision abrasive waterjet cutting”, in H. Louis (Ed.), Proceedings of the 14th International Conference on Jetting Technology, Brugge, Belgium, September 21-23, pp 253-269.

Groppetti, R., & Monno, M. (1992) “A contribution to the study of burr formation in hydro abrasive jet machining”, in A. Lichtarowicz (Ed.), Jet Cutting Technology - Proceedings of the 11th International Conference on Jet Cutting Technology, St Andrews, Scotland, September 8-10, pp 621-633.

Hashish, M. (1984) “On the modeling of abrasive-waterjet cutting”, in G.A. Watts & J.E.A. Stanbury (Ed.), Proceedings of the 7th International Symposium on Jet Cutting Technology, June 26-28, Ottawa, Canada, pp 249-265.

Hashish, Mohamed (2007) “Benefits of dynamic waterjet angle compensation”, in Mohamed Hashish (Ed.), Proceedings of the 2007 American WJTA Conference and Expo, Houston, Texas, USA, August 19-21, Paper 1-H.

Henning, Axel (1997) “Computer aided manufacturing for three-dimensional abrasive water jet machining”, Proceedings of the 9th American Waterjet Conference , Volume II , Dearborn, Michigan, August 23-26.

Henning, A. & Anders, S. (1998) “Cutting-edge quality improvements through geometrical modeling”, in H. Louis (Ed.), Proceedings of the 14th International Conference on Jetting Technology, Brugge, Belgium, September 21-23, pp 321-328.

Henning, A., Goce, R., & Westkämper, E. (2002) “Analysis and control of striation structures at the cutting edge of abrasive waterjet cutting”, in Paul Lake (Ed.), Proceedings of the 16th International Conference on Jetting Technology, Aix-en-Provence, France, October 16-18, pp 173-191.

Henning, A. & Westkämper, E. (2006) “Analysis of the cutting front in abrasive waterjet cutting”, in Peter Longman (Ed.), Proceedings of the 18th International Conference on Water Jetting, Gdansk, Poland, September 2006, pp 425-434.

Henning, A. & Westkämper, E. (2007) “Dynamice analysis of the spatial-temporal behaviour of the cutting front in abrasive waterjet cutting”, in Mohamed Hashish (Ed.), Proceedings of the 2007 American WJTA Conference and Expo, Houston, Texas, USA, August 19-21, Paper 5-B.

Henning, A. & Westkämper, E. (2000) “Modelling of contour generation in abrasive water-jet cutting”, in Proceedings of the 15th International Conference on Jetting Technology, Ronneby, Sweden, September 6-8, pp 309-320.

Henning, A., Westkamper, E., & Schmidt, B. (2004) “Analysis of geometry at abrasive waterjet cutting operation”, In Colin Gee (Ed.), Proceedings of the 17th International Conference on Water Jetting -- Advances and Future Needs, Mainz, Germany, 7th - 9th September, pp 465-474.

Henning, Axel (2007) “Modellierung der Schnittgeometrie beim Schneiden mit dem Wasserabrasivstrahl”, Berichte aus dem Fraunhofer Institut fuer Produktionstechnik und Automatisierung, Nr. 470.

Kitamura, M., Ishikawa, M., Sudo, K., Tujita, K. (1992) “Cutting of steam turbine components using an abrasive water jet”, in A. Lichtarowicz (Ed.), Jet Cutting Technology - Proceedings of the 11th International Conference on Jet Cutting Technology, St Andrews, Scotland, September 8-10, pp 543-554.

Maccarini, G., Monno, M., Pellegrini, G., & Ravasio, C. (2008) “Characterization of the AWJ kerf: the influence of material properties”, in Proceedings of the 19th International Conference on Water Jetting, Nottingham, UK, October 2008, pp 67-76.

Matsui, S., Matsumura, H., Ikemoto, Y., Tsujita, K., & Shimizu, H. (1990) “High precision cutting method for metallic materials by abrasive waterjet”, in D. Saunders (Ed.), Jet Cutting Technology - Proceedings of the 10th International Symposium, Amsterdam, The Netherlands, October 31 - November 2, pp 263-278.

Olsen, John (2009) “Limits of Precision Cutting with Abrasive Waterjets”, submitted to the 9th Pacific Rim International Conference on Water Jet Technology, Koriyama, Japan, November 20 -23.

Westkämper, E., Henning, A., Radons, G., Friedrich, R., & Ditzinger, T. (2000) “Cutting edge quality through process modeling of the abrasive waterjet”, in Proceedings of the 2nd CIRP International Seminar, Capri, Italy.Neapel, June 21-23, pp. 179-188.

Zeng, J., Heines, R., & Kim, T.J. (1991) “Characterization of energy dissipation phenomenon in abrasive waterjet cutting”, in Proceedings of the 6th American Waterjet Conference, Houston, Texas, USA, August, 1999, pp 163-177.

Zeng, J., Kim, T.J., and Wallace, R.J. (1992) “Quantitative Evaluation of Machinability in Abrasive Waterjet Machining,” *Proceedings of the 1992 Winter Annual Meeting of ASME, “Precision Machining: Technology and Machine Development and Improvement,”* PED-Vol.58, pp. 169-179, Anaheim.

Zeng, J., Olsen, J., Olsen, C. and Guglielmetti, B. (2005) "Taper-free abrasive waterjet cutting with a tilting head", Proceedings of the 2005 American Waterjet Conference, Houston, Texas. August 21-23, Paper 7A-2.

7. NOMENCLATURE

A	coefficient
AM	abrasive mesh number
AR	abrasive mass flow rate
B	coefficient
C_1	coefficient
C_3	coefficient
e_x	unit vector in the direction of feed
h	workpiece thickness
J	a spatio-temporal model of the moving jet profile
KW	kerf width, measured at top of the kerf
MD	mixing tube diameter
P	water pressure
Q	quality index
r	radial coordinate of the jet
R_e	entrance radius
t	time
TA	taper angle, i.e. the arctangent of taper error over thickness
TE	taper error, i.e. half of the difference between the top and bottom kerf width
U	cutting speed
WR	water mass flow rate
λ	feed rate